A Clinical Decision Support System to Identify and Stage Breast Cancer Tumor

G. Norhene[1*], D. Alima[1], S. Dorra[1] and A. Riadh[2]

[1]Computer Imaging and Electronic System Group from the CEM Lab University of Sfax, Sfax Engineering School, Tunisia.
[2]El Farabi Radiology Center, Faculty of Medicine Sfax, Road Ahmed Aloulou, Building, El Farabi Sfax El Jadida, BP W, 3003 Sfax, Tunisia.

Authors' contributions

This work was carried out in collaboration between all authors. Author GN designed the study, performed the statistical analysis, wrote the protocol, and wrote the first draft of the manuscript. Authors DA and SA managed the analyses of the study. Author AR expert radiologue collaborate in the diagnosis of breast cancer and analysis of mammographic images. All authors read and approved the final manuscript.

Original Research Article

ABSTRACT

Aims: An improved Clinical Decision Support System is developed to classify the tumor and identify the different stages of the breast cancer.
Methodology: In this paper, we analyze and compare the performance of a developed system that takes the breast density information into account. The advantages of consideration of this breast density information will be highlighted. Our proposal is based on multi-resolution Gray Level and Local Difference (GLLD) for feature extraction. Once the descriptors are extracted, Artificial Neural Network (ANN) are used for classifying the detected masses according to their corresponding stages.
Results: The accuracy of the proposed system has been verified and found that the Area Under the Curve (AUC) of 99.5% can be achieved for tumor staging when considering the information of beast density and applying the multi-resolution GLLD as texture descriptor. The proposed system may provide valuable information concerning cancer staging.

Keywords: Breast density; artificial neural network; cancer staging, multiresolution gray level and local difference.

_____

*Corresponding author: Email: norhene.gargouri@live.fr;

1. INTRODUCTION

Breast cancer is still considered as a major health problem. Early detection of malignancy can potentially ameliorate breast cancer prognoses and it may also reduce female mortality. Radiologists rely heavily on computer-aided detection/diagnosis systems (CAD) which are very helpful in the breast lesion detection and classification [1,2]. These systems are referred as CADe systems; whereas computer-aided diagnosis system as CADx systems. Because the automated mammogram lesions interpretation is still delicate, the development of reliable and robust CAD systems is of great importance. Which renders the issue more complicated is presence of dense breast tissue. The latter may make suspicious areas almost invisible and leads to its misinterpreted as calcifications or masses [3,4]. In [5,6], interest has been focused on investigating breast tissue density since wolfe discovered [7], the link between mammographic parenchymal patterns and the risk of developing breast cancer. There exist a lot of research articles describing epidemiological studies such as breast cancer risk estimation [8], and diagnosis support by content-based retrieval [9,10] that is based on tissue density information. Thus, our research focuses on the classification of breast tissues. It, also, reaches around the development of CAD algorithms for breast lesions automated analysis. Recent studies have proven that if the breast density information is considered, the CAD system performance is improved [11,12].These studies demonstrate a CAD system total sensitivity of 88.5% with an accuracy of 78%. In density type 3 and 4, the CAD's sensitivity was usually low. In masses having density 3, the specificity was 79%; whereas, it was 45% in those with density 4. For microcalcification present in the density four types and for masses having density 1 and 2, the specificity was up to 80%. Therefore, adjusting the lesion detection algorithm input parameters is necessary to control its sensitivity, which depends on the type of tissue to reduce false-positive detections, especially in dense tissue, at the same detection rate.

Several studies concerned with the breast tissue classification have been detailed in the literature [13]. According to the American College of Radiology BIRADS [14] the images are divided into four categories: The first one is entirely fat, its glandular tissue is less than 25%. For T. II breast density, there exist scattered fibroglandular tissues which range from 25 to 50% of the breast. Dense tissue in T. III varies from 50 to 75%. The final category of breast density means that the breast has more than 75% glandular and fibrous tone. The characteristics utilized for the classification process are based on texture information. The most efficient features for characterization are extracted from the histogram of gray level and the patters of texture [15]. Some studies have shown that the information of histogram alone is not sufficient to classify mammograms according to the categories of BIRADS [16].

The remaining part of this article is organized as follows: The second section presents the problem overview in the literature. Section 3 shows the methods and materials utilized in this work. These consist of feature extraction procedure, the statistical analysis, the tested classifiers, the testing procedure and the training one, and the used experimental database. In section 4, we explain the classifiers integration into the CADe and the implementation of the system. Availability mode and system requirements are illustrated in the fifth section. Section 6 shows the obtained results with the proposed methods. Section 7 presents brief conclusions.

2. MATERIALS AND METHODS

2.1 Effect of Density Pattern on the Estimation of Cancer Stage

Breast density is estimated according to the conventional BIRADS categories [17].

- BIRADS I: Generally entirely fatty breast
- BIRADS II: Presence of some fibroglandular tissue
- BIRADS III: Heterogeneously dense breast tissue
- BIRADS IV: Extremely dense breast tissue

Fig. 1 illustrates the flow diagram of the proposed system.

Texture features are extracted using the LBPV approach from the different tissues and used to characterize mammograms. These mammograms are then classified according to the conventional BIRADS categories using the ANN classifier.

2.1.1 Feature descriptor

The local binary pattern (LBP) is an operator transforming the input data into an image of integer labels which describe small-scale appearance of the image. These labels, most frequently the histogram, are then applied for image analysis. The local binary pattern operator, introduced in 1996 by Ojala et al. [18], was based on the hypothesis that texture has two complementary aspects, the pattern and its corresponding strength.

The original version of the LBP operator was applied in a 3×3 . block of an image. The pixels of this block were first thresholded by the value of the central pixel, then they were weighted by powers of two and finally summed to obtain the label for the central pixel.

For each block, the neighborhood consists of 8 pixels. So, a total of 2^8 labels may be obtained depending on the value of the pixels of the neighborhood.

The original version of the LBP was extended in a new generic revised form, then, in 2002 by Ojala et al. [19]. This Generic LBP Operator puts no limitations to the neighborhood size or to the sampling points number. The derivation of the generic LBP as detailed below follows that of Mâenpââ et al. in 2005 [20].

Let's consider an image I(x,y) and g_c the gray value of the pixel (x, y):

$$g_C = I(x, y)$$

(1)

Let g_p be the gray value of a sampling point in a circular neighborhood. P corresponds to the number of sampling points and R is the radius around the point (x, y):

$$g_p = I(x, y), \, p = 0,..., \, P - 1$$

(2)

$$x_p = x + R \cos(2\pi p) \tag{3}$$

$$y_p = y - R \sin(2\pi p) \tag{4}$$

The local texture of an image I(x,y) may be characterized by a joint distribution of the gray values of p+1 pixels:

$$T = (g_c, g_0, g_1, ..., g_{P-1}), P > 0 \tag{5}$$

The center pixel value may be subtracted from the neighborhood as follows:

$$T = (g_c, g_0 - g_c, g_1 - g_c, ..., g_{P-1} - g_c) \tag{6}$$

Furthermore, the joint distribution may be approximated by estimating the center pixel statistically independent of the obtained differences; this allows a factorization of the distribution:

$$T \approx (g_c) t(g_0 - g_c, g_1 - g_c, ..., g_{P-1} - g_c) \tag{7}$$

$t(g_c)$ corresponds to the intensity distribution of I(x,y). Thus, the joint distribution of differences may be noted as:

$$T \approx t(g_0 - g_c, g_1 - g_c, ..., g_{P-1} - g_c) \tag{8}$$

Only the signs of the differences are considered to define the LBP code:

$$T \approx t(s(g_0 - g_c), s(g_1 - g_c), ..., s(g_{P-1} - g_c)) \tag{9}$$

$s(z)$ corresponds to the thresholding, it is defined as:

$$s_z = \begin{cases} 1, z >= 0 \\ 0, z < 0 \end{cases} \tag{10}$$

The LBP operator was derived from the obtained joint distribution. As in the case of the basic LBP, it was obtained by summing the differences multiplied by powers of two.

So, the $LBP_{P,R}$ operator is defined as:

$$LBP_{P,P}(x_c, y_c) = \sum_{p=0}^{P-1} s(g_p - g_c) 2^p \tag{11}$$

The signs of the differences in each neighborhood is a P bit binary number, 2^P is distinct values in the lbp code. Therefore the texture, is so approximately described with 2^P bin discrete distribution of the LBP codes:

$$T \approx t(LBP_{P,R}(x_c, y_c))$$

(12)

The $LBP_{P,R}$ operator produces 2^P output values corresponding to 2^P different local binary patterns that may be assembled by P pixels in the neighborhood. During image rotation, g_p will move around g_c. It is generally assigned to be the value of the central element (0,R). The rotation of a binary pattern results in a new $LBP_{P,R}$ value but this is not true for patterns composed only of 0's or 1's. To remove rotation effect, we define [20]:

$$LBP_{P,R}^{ri} = \min\left\{ ROR(LBP_{P,R}, i) \mid i = 0,1,..., P-1 \right\}$$

(13)

Where ROR(x,i) achieves a circular right shift on the bit P with a value x, i times. For image pixels, this corresponds to the rotation of the neighbor set clockwise. $LBP_{P,R}^{ri}$ quantifies the occurrence statistics of individual rotation invariant patterns which correspond to certain micro-features in the image. Thus, the patterns may be considered as feature detectors.

The $LBP_{8,R}^{ri}$ may have 36 different values. For example, patterns in which LBP value is 0 corresponds to a bright spot.

The LBP code for each neighborhood is formed and its decimal values are computed. They represent local information of texture. Black and white circles correspond respectively to bit values of 0 and 1.

We may notice that certain local binary patterns correspond to fundamental properties of texture, providing vast majority of all 3.3 patterns presented in the textures. These fundamental patterns are called "uniform".

To define the "uniform" patterns, we introduce the uniformity measure $U(LBP_{P,R})$. This latter corresponds to the number of spatial transitions in the pattern.

We designate patterns that have $U(LBP_{P,R})$ value at most 2 as "uniform" and we propose the following operator instead of $LBP_{P,R}^{ri}$.

$$LBP_{P,R}^{riu2} = \begin{cases} \sum_{p=0}^{P-1} \left| s(g_p - g_c) \right| if \quad U(LBP_{P,R}) <= 2 \\ P+1 \, otherwise \end{cases}$$

(14)

Where

$$U(LBP_{P,R}) = \left| s(g_{p-1} - g_c) - s(g_0 - g_c) \right| + \sum_{i=1}^{P-1} \left| s(g_p - g_c) - s(g_{P-1} - g_c) \right|$$

(15)

The supersript $^{riu\,2}$ reflects the use of the rotation invariant uniform patterns that have $U(LBP_{P,R})$ value at most 2.

$\dfrac{LBP_{P,R}^{riu2}}{VAR_{P,R}}$ is a local contrast information descriptor of exploiting the complementary features of local spatial patterns and contrast [21].

High frequency textural information regions usually have higher variances; they contribute more to the image discrimination. Thus, LBPV presented to characterize the local contrast information into a one-dimensional LBP histogram in which $VAR_{P,R}$ is used as an adaptive weight to adjust the LBP descriptor contribution in histogram calculation.

The local binary variance code histogram is calculated as follows:

$$LBPV_{P,R} = \sum_{i=1}^{N} \sum_{j=1}^{M} \omega(LBP_{P,R}^{riu\,2}(i,j),k), k \in [0, K]$$

(16)

$$\omega(LBP_{P,R}^{riu\,2}(i,j),k) = \begin{cases} VAR_{P,R}(i,j), & LBP_{P,R}^{riu\,2}(i,j)=k \\ 0 \; otherwise \end{cases}$$

(17)

Although LBP operator is locally operated; it has a good ability to summarize the different global or local densities in the image. Fig. 2 demonstrates such ability. As shown, each density in a mammogram image can be presented by a different mammogram. Thus, LBPV is considered as a good descriptor candidate that can ultimately handle the different densities in the mammographic images.
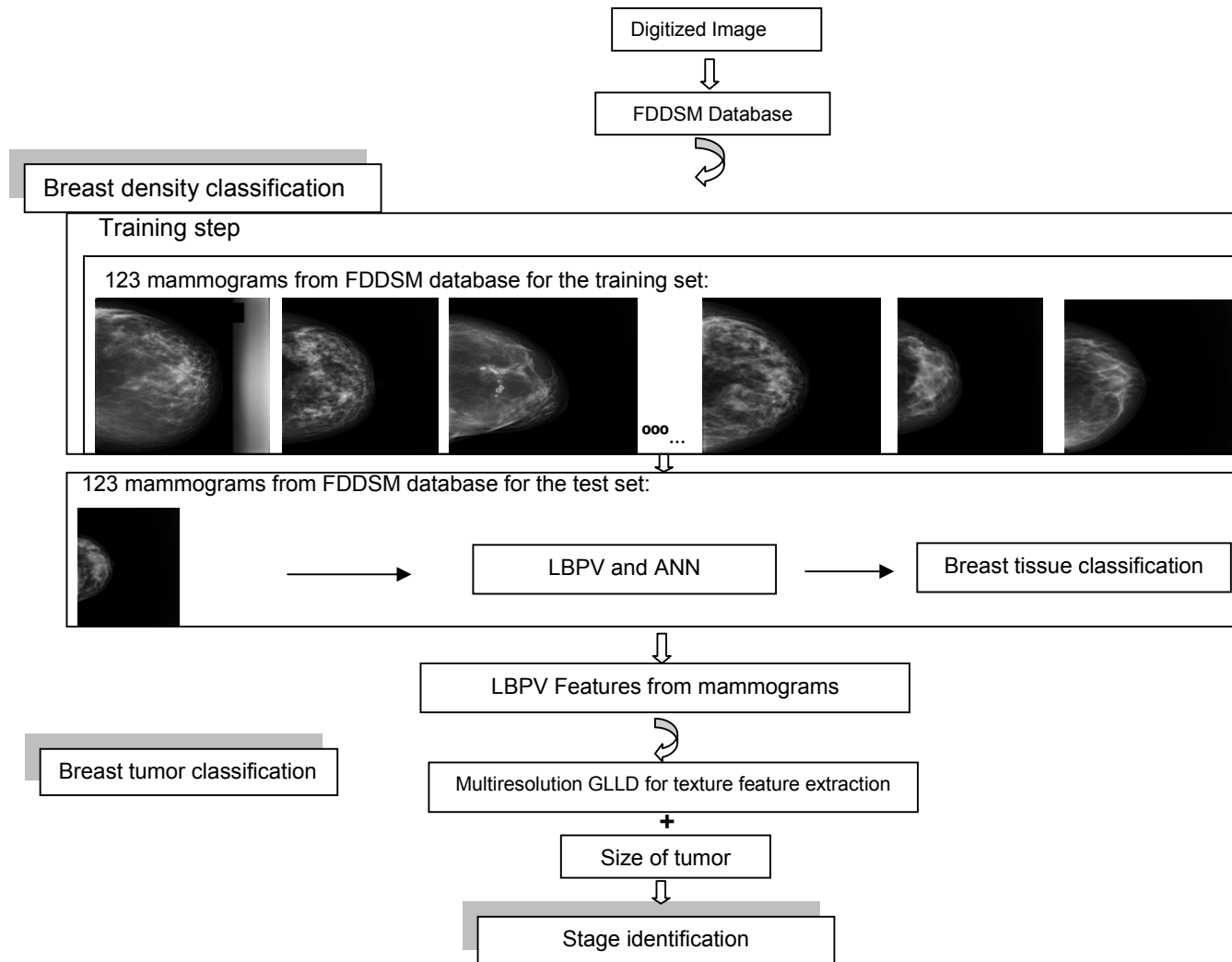
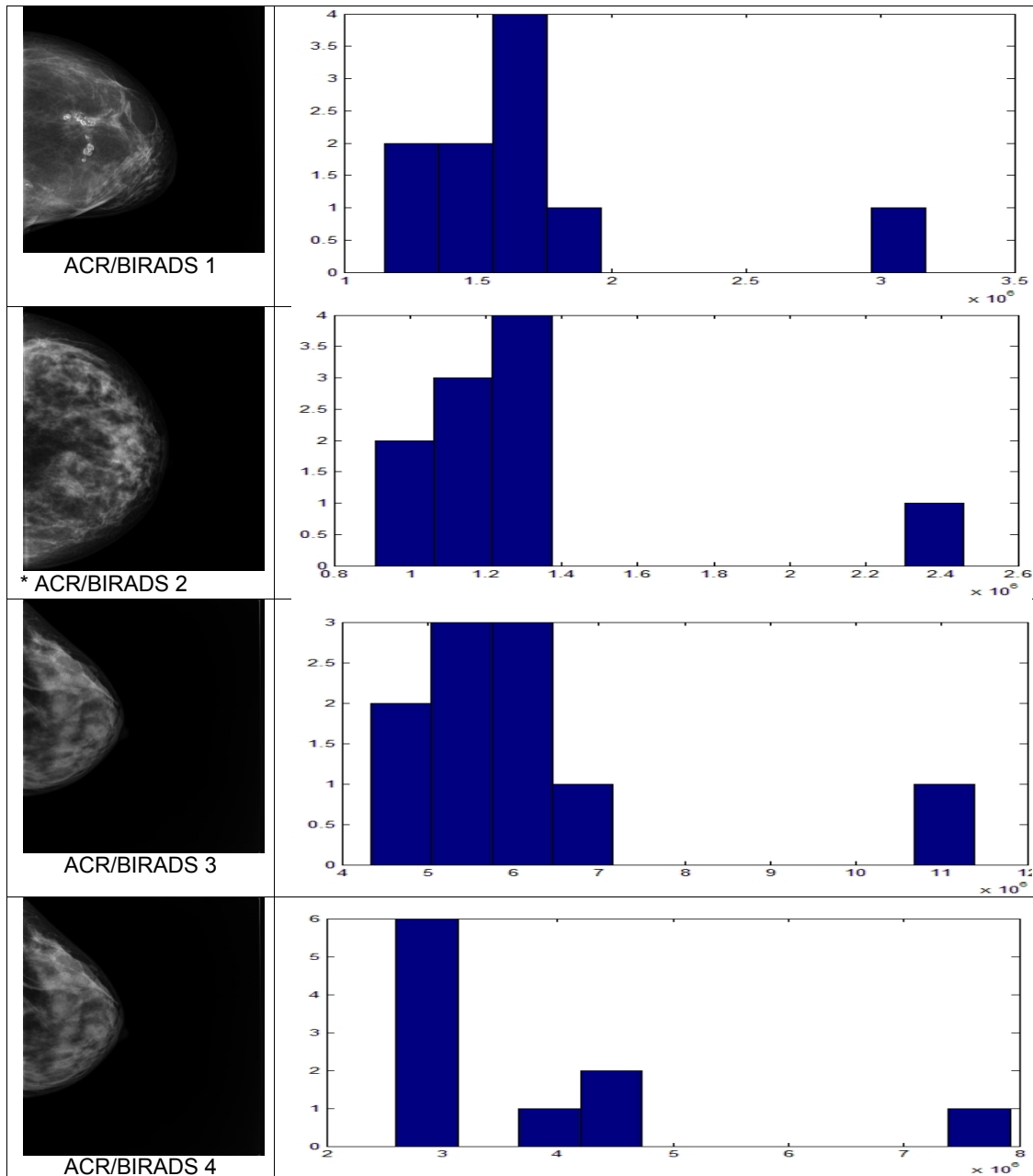**Fig. 1. The proposed methodology for tumor classification and stage identification**

Fig. 2. Density classification of samples from FDDSM database

2.1.2 Classification module

Usually, the ANN is viewed as system information composed of interconnected elements that consist a network. Its main function is to adjust weights between neurons.

If $x = (x1, x2,..., xd)^T$ is an input vector and $\omega = (\omega1, \omega2,..., \omega d)^T$ the weight vector, so the output is computed as follows:

$$y = g(\omega^T x_b) = g(\sum_{i=1}^{d} \omega_i x_i - b)$$

(18)

Where g (.) is specifically a sigmoïdal activation function presented by:

$$g(x) = (1 + e^{-x})^{-1}$$

(19)

Table 1. Target of the ANN

Output	Y4	Y3	Y2	Y1
ACR/BIRADS I	0	0	0	1
ACR/BIRADS II	0	0	1	0
ACR/BIRADS III	0	1	0	0
ACR/BIRADS VI	1	0	0	0

We calculate the LBPV vector for each mammogram. These features are then utilized as neural network inputs in the classification stage.

To evaluate the training effectiveness, we measure the error by the following equation:

$$E = \frac{\sum_{i=1}^{n} (I_N - I_T)}{number \quad of \quad samples}$$ ……………………………………………………………………….(20)

Where I_N is the image which results from ANN output; whereas I_T is the target. After the training steps, generalization error is evaluated according to different features and network conditions. Table 2 presents the details of the MLP network.

Table 2. Characteristics of the ANN

Activation function	Sigmoid function
Hidden layer	1
Number of hidden units	20
Input neurons	512
Output neurons	1
Number of iterations	10000

Once the stage of tissue classification is done, the density of the breast is automatically estimated. The following CAD system is considered with the aim to take the obtained breast density into account, thus this is accomplished by classifying the initial database according

to breast density estimation. When a mammogram is analyzed, density information may be attained from:

1. Manual annotation delineated by a radiologist.
2. Automatic estimation, in this case mammogram density is estimated by the algorithm explained previously.

These strategies are compared in the experimental section. For most cases, automatic estimation agrees with expert annotation, but in this analysis, we will present the main differences in CAD performances when using manual and automated automatic breast density estimation.

2.2 Identification of the Stages of Cancers

2.2.1 Estimation of tumor growth

The various stages of cancer may be distinguished by the growth of tumor size [22]. The tumor stages are identified from stage 0 to stage 4.

Stage 0: This stage depicts non-invasive breast cancer, representing no confirmation of cancer cells.
Stage 1: This stage characterizes the tumor at its initial growth; in this case the cell multiplication rate is slower. The tumor size is less than 20mm.
Stage 2: The tumor size is between 20 and 60mm. Here the development of the tumor is relatively vigorous than the former stage, the cell multiplication is at a rapid progress.
Stage 3: The tumor size is larger than 60 mm and can be attached to the surrounding structures. The growth rate of the tumor in this stage is very quick.
Stage 4: Tumor of any size growing into the chest wall or skin. This includes inflammatory breast cancer.

From the Fig. 3 it is noticed that, the various stages are measured depending on the size of the tumor. If the tumor size is less than 20mm, it is considered in the initial stage (stage 1). The tumor of size among 20–60mm is considered as prudence (stage 2). The tumor of size between 60–80mm is considered as dangerous tumor (stage 3).The increase of the size of the tumor above 80mm is a sign of emergency (stage 4).

2.2.2 Principle of the multiresolution GLLD

The major disadvantage of the GLLD is its limited spatial support area. Features computed in the local 3×3 neighborhood cannot capture the large-scale structures that may be dominant features of most of the textures. Nevertheless, the obtained GLLD codes are not absolutely independent of each other. Each GLLD code limits the set of its adjacent codes, making the area of the single code slightly larger than 3×3 pixels. Thus, the operator is not so robust against the local changes in produced texture. Thus, for the discrimination of the tumor stage we need a new operator presenting a larger spatial support area is needed.

A simple, yet efficient way to enlarge the spatial support area is the combination of the obtained information by N GLLD operators while varying P and R values. Therefore, each pixel in the texture image gets as input N different GLLD codes. The concatenation provides the most accurate information.
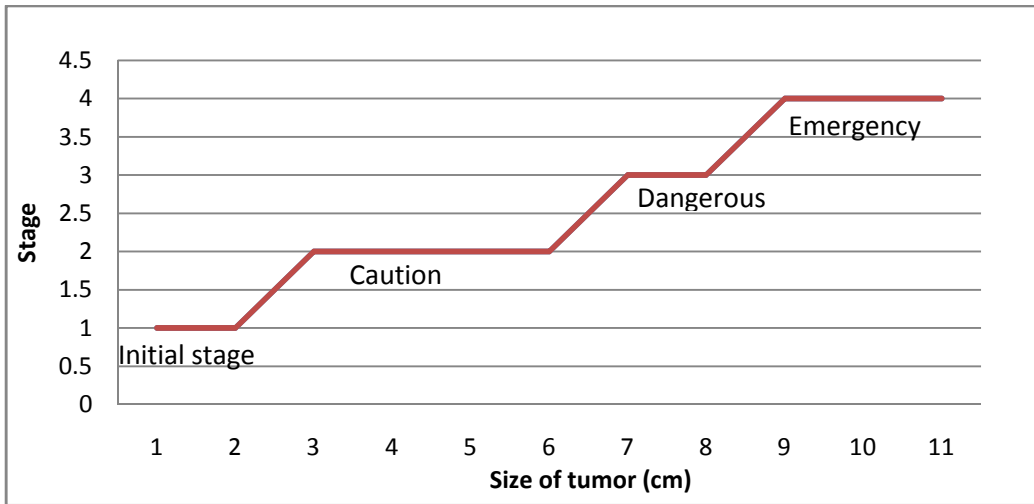
Fig. 3. Size of tumor through various stages

The GLLD [23] is based on three proposed types of features. The proposed image is presented as the central gray level and the local difference. The attained local difference is decomposed into two components as follows:

$$diff_p = m_p s_p \tag{16}$$

where the first component corresponding to the sign component is computed as follows:

$$.s_p = \begin{cases} 1, & diff_p \geq 0 \\ -1, & diff_p < 0 \end{cases} \tag{17}$$

and the magnitude component is computed as the modulus of the difference.

Consequently, three new operators named CGLLD, SGLLD and MGLLD were obtained. Then, the obtained codes were joined to form the final GLLD feature map. Finally, the obtained histogram can be built and the nearest neighborhood classifier is applied for texture classification.

The MGLLD operator is defined as:

$$MGLLD_{P,R} = \sum_{p=0}^{P-1} t(m_p, c) 2^P \tag{18}$$

$$t(x,c) = \begin{cases} 1, & x \geq c \\ 0, & x \prec t \end{cases} \tag{19}$$

However CGLLD is defined as:

$$CGLLD_{P,R} = t(g_{cmean}, c_I)$$

$$(20)$$

where c_I represents the threshold. It represents the mean gray level of the input texture image.

Each code carries specific information about the texture; we combined them and we obtain CGLLD feature. The rotational invariant CGLLD uniform version was applied.

In 2012 [23], we applied the GLLD for mass detection of mammographic images, According to the size of the lesion, we used six groups of Regions of interest (ROI) images, corresponding to the following mass sizes intervals: < 10 mm, (10−60) mm, (60−120) mm, (120−190) mm, (190−270) mm,> 270mm. The number of masses in each interval was 28, 32, 37, 57, 69, and 33, respectively. Note we are dealing with different lesion sizes, an important aspect for correctly classifying the masses. The proposed approach leads to good results, however, we want to clarify that our approach outperforms in cases of masses with size lower than 120 mm. To overcome this limitation, we propose in this paper to extend the GLLD approach to a multi-resolution version knowing that multi-resolution analysis allows to exploit additional discriminant information. Fig. 4 shows an example of segmented ROIs generated by the experienced radiologists.
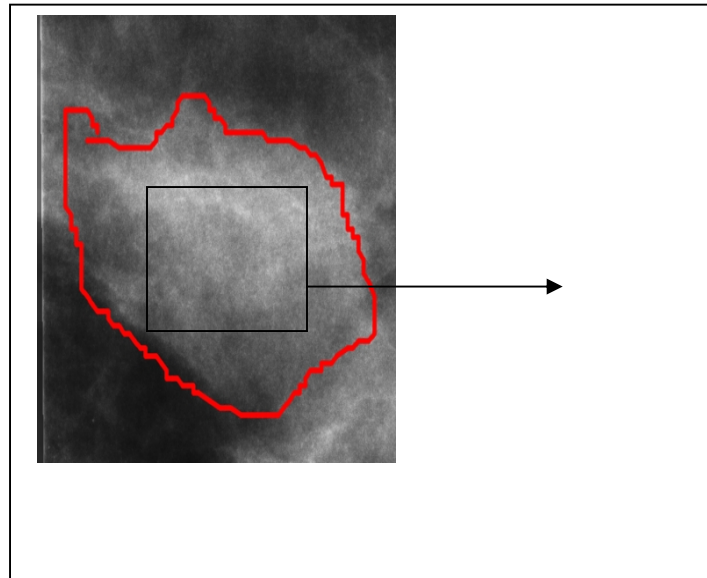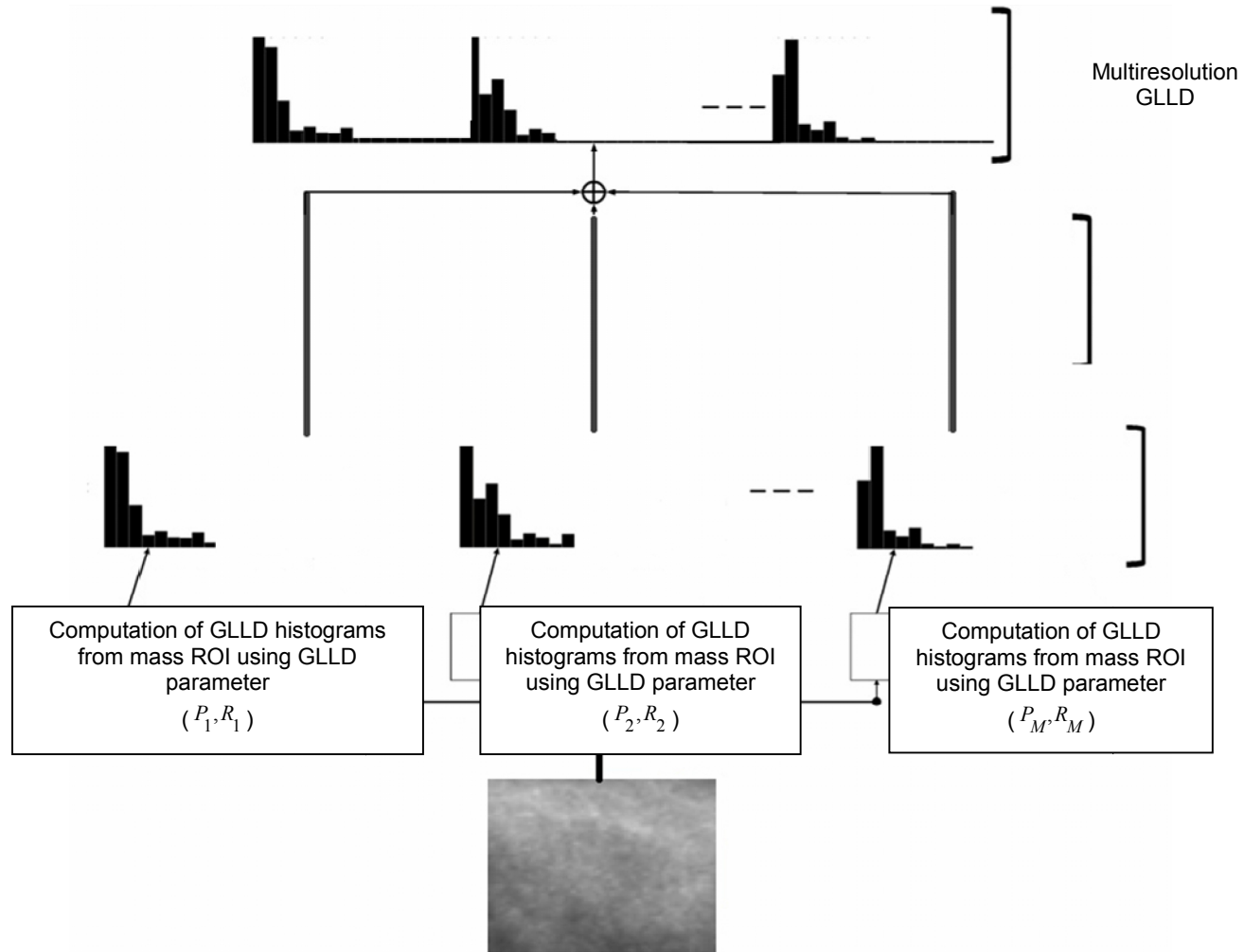

Fig. 4. Mass ROI

Fig. 5. Illustration if the principle of the multiresolution GLLD

3. RESULTS AND DISCUSSION

The images from FDDSM database [24] and from DDSM database [25] have been considered in the development of the decision system. Results have been divided in two main classes, one evaluating density classification and other evaluating the results of breast cancer staging with consideration of breast tissue classification cancer staging with consideration of breast tissue classification.

3.1 Density Classification Results

The proposed approach correctly marked 94% (115/123) of mammogram density. LBPV and ANN correctly marked 100% of cancers in fatty breasts, 95% of cancers in breasts containing scattered fibroglandular densities, 93% of cancers in heterogeneously dense breasts, and 60% of cancers in extremely dense breasts. Table 3 presents the confusion used to tabulate the true positive, false positive, true negative, and false negative rates for a classifier. These results are summarized in Table 4.

Table 3. A confusion used to tabulate the true positive, false positive, true negative, and false negative rates for a classifier

	Belonging to the BI-RADS category in question	Belonging to BIRADS category
positif test	True positives	False positives
Negatif test	False negatives	True negatives

Table 4. Automatic BI-RADS Breast Density classification

BI-RADS breast density	Results of classification		
BIRADS I		belonging to BI-RADS I	not belonging to BI-RADS I
	positif test	6	0
	Negatif test	0	0
BIRADS II		belonging to BI-RADS II	not belonging to BI-RADS II
	positif test	63	.0
	Negatif test	2	0
BIRADS III		belonging to BI-RADS III	not belonging to BI-RADS III
	positif test	43	1
	Negatif test	3	0
BIRADS IV		belonging to BI-RADS IV	not belonging to BI-RADS IV
	positif test	3	0
	Negatif test	2	0

3.2 Influence of Taking Breast Density into Account for Final Classification of Rois

The performance of this system has been evaluated in terms of sensitivity and specificity. The sensitivity corresponds to the probability that a diagnostic test is positive, given that the

person has the disease. Specificity corresponds to the probability that a diagnostic test is negative, given that the person does not have the disease [21]. The Receiver Operating Characteristic (ROC) is a plot of sensitivity against (1—specificity). The texture features have been given as input to the multilayer back propagation neural network for classification. The area under the ROC (AUC) curve is an important parameter to determine the overall classification accuracy in the different stages of the proposed system.

The FDDSM database is composed by normal and abnormal cases; we use the ROC curve, which has been proven to provide a more robust analysis in such cases [26]. In Fig. 6, we obtained an AUC 0.93 without considering breast density information and 0.99 when using automatic density annotations The use of breast density information significantly increases the performance of the proposed system, and the use of automatic density estimation outperforms the use of manual annotations.
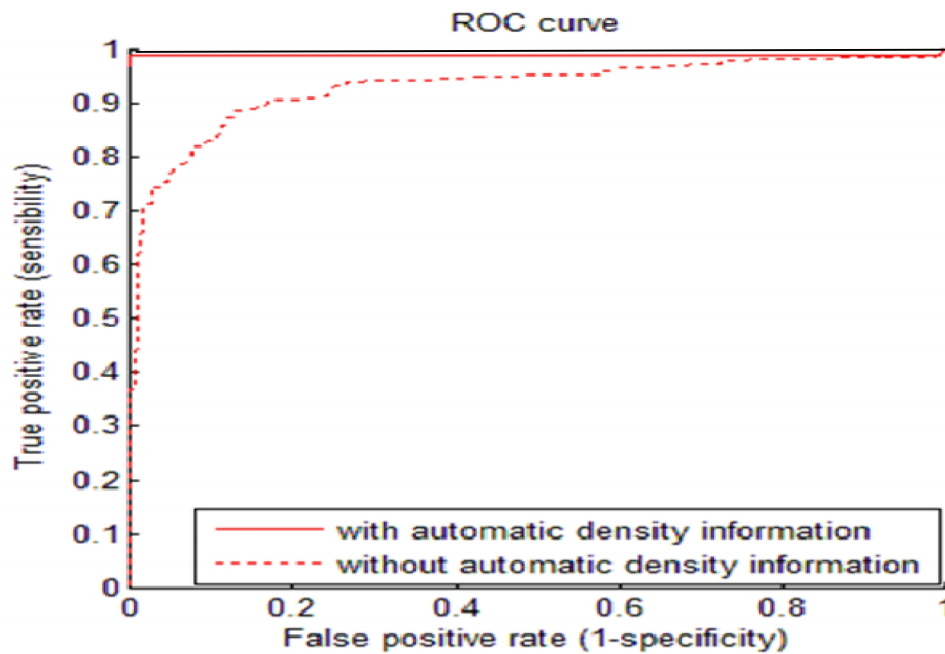

Fig. 6. ROC curve

It should be clear that the inclusion of the information of breast density increases the detection rate for all mass sizes. The advantage of taking breast density into account may be explained by analyzing the new detected masses when considering this additional information. In fact, for mammograms of low density, some masses are not detected because they are confused as accumulations of a dense tissue, so training with only cases of low density avoids this confusion.

However, for mammograms of high density, on the one hand, the system learns that masses edges are more subtle than edges in the cases of fatty mammograms. On the other hand, the training is restricted to dense mammograms, so the system is able to distinguish some masses with low contrast that otherwise may be missed.

Table 5. Results of cancer staging

Size of the Tumor(mm)	Database	Size1: <20	Size2: (20-60)	Size3: (60-120)	Size4: (120-190)	Size5: (190-270)	Size6:>270	Mean
Stages		**1**	**2**	**3 and 4**				
• Oliver et al. [7]	DDSM	0.53	0.7	0.7	0.68	0.72	0.83	0.7
• Oliver et al. [8]	DDSM	0.81	0.83	0.87	0.84	0.89	0.93	0.86
• Gargouri et al. [4]	DDSM	0.98	0.99	0.97	0.92	0.93	0.9	0.94
• $GLLD_{8,1+16,2+24,3} + ANN$ (with automatic density information)	FDDSM	0.97	0.99	0.95	**0.97**	**0.99**	**0.96**	**0.97**
• $GLLD_{8,1+16,2+24,3} + ANN$ (with automatic density information)	DDSM	0.96	0.92	0.93	0.96	**0.97**	0.99	**0**.95
• Expert Radiologist	DDSM	0.80	0.76	0.82	0.93	0.92	0.95	0.86

3.3 Results of Cancer Staging

Table 5 above illustrates the results of mass classification when applying the proposed system with breast density information. In our previous studies [4], the obtained AUC for some mass sizes was less than 0.9, so, the system previously developped, allows a good detection of mass versus non-mass but it is not able to classify these masses according to their sizes properly. In Table 5 we present a comparison of our technique with another work to prove that our method is better than the other. The comparison is based on area under roc curve (Az). All compared studies use publicly available image databases. It's obvious that for the public and local database used, this methodology proves robust and generic classification of ROI's into mass class non-mass one, and promotes the reduction of false positives. For instance, the works of Oliver et al. [25] obtained Az values of 0.7 and 0.86 respectively. We notice that better performances were clearly obtained using our proposal. Consequently, it is generally difficult to define a priori universal resolution for the ROIs to be used for texture analysis. However, it may be expected that the multi-resolution analysis is beneficial when dealing with the aforementioned problem because it could provide a scale-invariant interpretation of the proposed region of interest. The multiresolution analysis with consideration of the information of breast density allows to improve the detection rate for some cases of masses with size >120mm.

The ANN with more weights model has a more complex function, and is therefore prone to over-learning for train test. Then it's important to present effectiveness (AUC) of the model for the train set (123 samples) and for the test set (123 samoles), separately. However, we want to clarify that all the methods used the same databases, and, therefore, our aim is to provide a general view of the different systems performance.

There are some aspects we would like to bring attention to. The first aspect is the computational cost of the different experiments. If we take into consideration the breast density information, the system computational time does not increase considerably. The second aspect is the data applied to test the proposed system. According to the size of the mass lesion, we classify them into six groups of Regions of Interest (ROI) images, corresponding to the previously mentioned mass size intervals. The number of masses in each size was 28, 32, 37, 57, 69, and 33, respectively. The final decision on different categories is confirmed by expert radiologists. This latter is satisfied of the results obtained when using the proposed system. The latter provides a "second read" of the mammogram to support the radiologist's interpretation.

4. CONCLUSION

The computer aided diagnosis system to identify the stages of cancer has been developed and validated with various samples. It is concluded from the analysis that the use of the breast density information is a significant factor to improve the results of classification of tumor. Further, it is seen that the stages of the breast cancer can also be predicted using the Information of the proposed system based on the multi-resolution GLLD descriptor. Based on our experimental results, the proposed feature extraction has proven to be significant for the purpose of FP reduction in the different mass size. Thus, this proposes system could considerably improve radiologists' accuracy in the characterization of breast tumor and in the identification of the stage of cancer.

ACKNOWLEDGEMENT

COMPETING INTERESTS

Authors have declared that no competing interests exist.

REFERENCES

1.   Birdwell R. The preponderance of evidence supports computer-aided detection for screening mammography, Radiology. 2009;253:9–16.
2.   Bueno G. Fuzzy systems and deformable models, series in medical physics and biomedical engineering, in: Intelligent and Adaptive Systems in Medicine, Taylor and Francis Group, London. 2008;10:305–329.
3.   Zhou C, Chan H, Petrick N, Helvie M, Goodsitt M, Sahiner B, Hadjiiski L. Computerized image analysis: Estimation of breast density on mammograms, Medical Physics. 2001;28:1056–1069.
4.   Brem R, Hoffmeister J, Rapelyea J, et al. Impact of breast density on computer-aided detection for breast cancer, American Journal of Roentgenology. 2005;184:439–444.
5.   Boyd NF, Byng JW, Jong RA, Fishell EK, Little LE, Miller AB, Lockwood GA, Tritchler DL, Yaffe MJ. Quantitative classification of mammographic densities and breast cancer risk: Results from the canadian national breast screening study, Journal of the National Cancer Institute. 1995;87:670–675.
6.   Sandberg M, Li J, Hall P, Hartman M, dos Santos-Silva I, Humphreys K, Czene K, Change of mammographic density predicts the risk of contralateral breast cancer: A case–control study, Breast Cancer Research. 2013;15(4):R57.
7.   Carney P, Miglioretti D, Yankaskas B, Kerlikowske K, Rosenberg R, Rutter C, Geller B, Abraham L, Taplin S, Dignan M, Cutter G, Ballard-Barbash R. Individual and combined effects of age, breast density, and hormone replacement therapy use on the accuracy of screening mammography. Annals of Internal Medicine. 2003;138(3):168–175.
8.   De Oliveira JE, Machado A, Chavez GC, Lopes A, Deserno TM, Araújo A. Mammosys: A content-based image retrieval system using breast density patterns. Computer Methods and Programs in Biomedicine. 2010;99:289–297.
9.   Ojala T, Pietikäinen Mäenpää M. Multiresolution gray-scale and rotation invariant texture classification with local binary patterns. IEEE Trans. Pattern Anal. Mach. Intell, 2002;24(7):971--987.
10. Mäenpää T, Pietikäinen M: Texture Analysis with Local Binary Patterns. In: Chen CH, Wang PSP (eds.): Handbook of Pattern Recognition and Computer Vision, 3rd edn. World Scientific. 2005;197-216.
11. Deserno TM, Soiron M, De Oliveira JE, Araújo A. Towards computer-aided diagnostics of screening mammography using content-based image retrieval, in: Lewiner T, Torres R (Eds.), Sibgrapi, (XXIV Conference on Graphics, Patterns); 2011.
12. Romero C, Varela C, Cuena R, Almenar A, Pinto J, Botella M. Impact of mammographic breast density on computer-assisted detection (CAD) in a breast imaging department, Radiologia. 2011;54(5):456–461.
13. Bovis K, Singh S. Classification of mammographic breast density using a combined classifier paradigm, in: 4th Intern. Workshop on Digital Mammography. 2002;177–180.

14. Breast Imaging Reporting and Data System Atlas (BIRADS), ACR, Reston, VA; 2003.

15. Wang XH, Good WF, Chapman BE, Chang YH, Poller WR, Chang TS, Hardesty LA. Automated assessment of the composition of breast tissue revealed on tissue-thickness-corrected mammography, American Journal of Roentgenology. 2003;180227–262.

16. Zhou C, Chan H, Petrick N, Helvie M, Goodsitt M, Sahiner B, Hadjiiski L. Computerized image analysis: Estimation of breast density on mammograms, Medical Physics. 2001;281056–1069.

17. Oliver A, Lladó X, Freixenet J, Martí R, Pérez E, Pont J, Zwiggelaar R. Influence of using manual or automatic breast density information in a mass detection CAD system. Academic Radiology. 2010;17(7):877-883.

18. Ojala T, Pietikäinen M, Harwood D. A comparative study of texture measures with classification based on feature distributions. In: Pattern Recognit. 1996;51-59.

19. Dammak Masmoudi A, Gargouri N, Sellemi Masmoudi D, Abid R. LBPV descriptors-based automatic ACR/BIRADS classification approach. Eurasip J. Image and Video Processing, Springer. 2013;19.

20. Alarcon T, Byrne HM, Maini PK. A multiple scale model for tumor growth. Multistage Model Simul. 2005;3(2):440–475.

21. Ojala T, Pietikâinen M, Mâenpââ TT. Multiresolutiongray-scale and rotation invariant texture classification with local binary pattern, IEEE Transactions on Pattern Analysis and machine intelligence. 2002;24(7):971-987.

22. Gargouri N, Dammak Masmoudi A, Sellemi Masmpoudi D, Abid R. 'FDDSM: Toward a Full Field Digital Mammographic Database', World Symposium on Computer Applications and Research, Sousse, Tunisia; 2014.

23. Available: http://marathon.csee.usf.edu/Mammography/Database.html.

24. Dammak Masmoudi A, Gargouri N, Sellemi D, Masmoudi Abid R. LBPV descriptors-based automatic ACR/BIRADS classification approach. Eurasip J. Image and Video Processing, Springer. 2013;19.

25. Oliver A, Martí J, Martí R, Bosch A, Freixenet J. A new approach to the classification of mammographic masses and normal breast tissue. IAPR Int Conf Pattern Recognit. 2006;4:707-10.

26. Birdwell R. The preponderance of evidence supports computer-aided detection for screening mammography, Radiology. 2009;253:9-16.

Peer-review history:
The peer review history for this paper can be accessed here:
http://www.sciencedomain.org/review-history.php?iid=572&id=32&aid=5004